Journal of Applied and Computational Mechanics, Vol. 3, No. 2, (2017), 114-124
DOI: 10.22055/jacm.2017.21276.1097

Journal of
Applied and Computational Mechanics

Analytical Investigations of the Effects of Tool Pin Profile and Process Parameters on the Peak Temperature in Friction Stir Welding

M. A. Waheed[1], L. O. Jaiyesimi[2], S. O. Ismail[3], O. U. Dairo[4]

[1, 3] Department of Mechanical Engineering, Federal University of Agriculture, Abeokuta, Nigeria.
[2]Works and Physical Planning Department, University of Lagos, Akoka, Lagos, Nigeria.
[4]Department of Civil Engineering, Federal University of Agriculture, Abeokuta, Nigeria.

Received February 19 2017; revised March 23 2017; accepted for publication April 02 2017.
Corresponding author: Lawrence Jayesimi, ljayesimi@unilag.edu.ng.

Abstract

In this work, effects of different tool pin profiles of flat and tapered shoulder geometries on the peak temperature in friction stir welding are investigated analytically. The developed models used for the analytical investigations considered the welding process as a combination or mixture of the pure sliding and the pure sticking. From the results, the amount of heat generation and the peak temperature are directly proportional to the number of edges in the pin profiles in such a way that the heat generated and peak temperature in the profiles increases from the triangular pin profile to hexagonal pin profile. Also, the rate of heat generation and the peak temperature in flat shoulder are greater than in tapered/conical shoulder. The results in this work are validated with experimental and the past theoretical results and good agreements are achieved.

Keywords: Frictional stir welding; Peak temperature; Different tool pin Profiles; Analytical investigations.

1. Introduction

The role of Friction stir welding (FSW) tool in the solid state welding process for the enhancement of weld quality and process efficiency has been well established. The understanding of the thermomechanical interaction in the welding is largely dependent on proper modeling of the heat generation and temperature history of the tool and workpiece. Consequently, several practical methods have been adopted to calibrate heat flow and temperature but none of these approaches enable the heat generation and weld temperature to be predicted without an experimental measurement of some kind. A more accurate and predictive approach uses the 3-dimensional flow field to calculate the heat generation from the material viscous dissipation. Even with these more sophisticated models, there is conjecture over the best ways to describe the material behaviour. Previous works on modeling the FSW process for heat generation from the FSW tool are based on assumptions regarding the interface condition, which led some limitations and inaccuracies. The fraction of heat generated by the probe is estimated to be as high as 20%, which leads to the conclusion that the analytical estimated probe heat generation contribution is not negligible. Also, the real situation during the welding process is a combination of the pure sliding and the pure sticking.

In the model by Chao and Qi [1] developed heat generation model based on the assumption of sliding friction, where Coulomb's law is used to estimate the shear or friction force at the interface. Also, in their model, the pressure at the tool interface is assumed to be constant, thereby enabling a radially dependent surface heat flux distribution as a representation of the friction heat generated by the tool shoulder, but neglecting the heat generated by the probe surface. Frigaard et al. [2] modeled the heat input from the tool shoulder and probe as fluxes on squared surfaces at the top and sectional planes on a three-dimensional model and control the maximum allowed temperature by adjustment of the friction coefficient at elevated temperatures. Russell and Shercliff [3] based the heat generation on a constant friction stress at the interface, equal to the shear yield stress at elevated temperature, which is set to 5% of the yield stress at room temperature. Gadash and Kumar [4] developed heat generation model for different pin

profiles in friction stir welding considering only sliding condition while Colegrove [5] uses an advanced analytical estimation of the heat generation for tools with a threaded probe to estimate the heat generation distribution. Raouache et al. [6] developed finite element simulation for transient three-dimensional thermal analysis of different tool geometries of the Friction stir welding using COSMOL MULTIPHYSICS while Emamikhah et al. [7], Ramanjaneyulu [8], Juarez et al. [9] presented out experimental studies on the role of pin profile and temperature on friction stir welding. Since the peak temperature attained during the welding process has direct effects on the microstructure and the control of peak temperature can potentially avoid the need for post-weld heat treatment for the welding of the material and to obtain defect-free joints. Therefore, the determination of the peak temperature is very important. However, the measurement of temperature at the stir zone is difficult due to intense plastic deformation and this pose a serious concern to researchers [10]. Therefore, Patil and Mastud [11] simulated the peak temperature in friction stir welding process of aluminium plates using COSMOL MULTIPHYSISC while Patel and Patil [12] simulated peak temperature and flow stress of aluminium alloy AA6061 for various tool pin profiles using finite element analysis software (HyperXtrude solver). Also, due to the fact that experimental measurements of large number of peak temperatures and cooling rates during FSW are time consuming and expensive [13].

A practical recourse has been based on the development of empirical model (an experimental data-based model) as done by Hamilton et al. [14] and Essa et al. [15]. However, the classical way for determining the peak temperature using mechanistic model is obviously still very important since it provides good insights into the significance of various welding parameters affecting the process. Therefore, in this work, effects of different tool pin profiles of flat and tapered shoulder geometries on the peak temperature in friction stir welding are investigated analytically. The developed models take into considerations that the welding process as a combination or mixture of the pure sliding and the pure sticking. The results in this work agreed with the conclusion of the past work. Therefore, the improved models could be used to estimate the heat generation in FSW tool.

2. Heat generation Models for different Pin and Shoulder Profiles

The pin geometry plays a vital role for material flow, temperature history, grain size, and mechanical properties in the FSW processes [4]. Therefore, heat generation models developed for different pin profiles with flat and conical shoulder has been developed in our previous paper [16] and they are given as:

(a) Triangular pin (b) Square pin (c) Pentagonal pin (d) Hexagonal pin

Fig. 1. Different profiles pin used in FSW [4]

2.1Triangular pin profile

The energy per unit length of the weld for the straight/flat shoulder tool is developed as

$$Q'_{Energy}=\frac{\omega\eta_{fd}}{vR_s^2}\left[\begin{array}{l}\frac{2}{3}\left[\mu F\left(R_s^3-\frac{a^3\sqrt{3}}{9}\right)(1-\delta_{st})+\tau_{yield}A_s\delta_{st}\left(R_s^3-\frac{a^3\sqrt{3}}{9}\right)\right]\\+\frac{2}{3}a^2\left[\frac{\sqrt{3}}{9}\mu Fa(1-\delta_{pt})+\frac{\sqrt{3}}{9}\tau_{yield}A_s\delta_{pt}\right]+\frac{1}{2\pi}a^2L_p\left[\mu F(1-\delta_{ps})+\tau_{yeild}A_s\delta_{ps}\right]\end{array}\right] \quad (1)$$

The energy per unit length of the weld for the tapered/conical shoulder tool is given as [16]:

$$Q'_{Energy}=\frac{\omega\eta_{fd}}{vR_s^2}\left[\begin{array}{l}\frac{2}{3}\left[\mu F\left(R_s^3-\frac{a^3\sqrt{3}}{9}\right)(1-\delta_{st})(1+tan\alpha)+\tau_{yield}A_s\delta_{st}\left(R_s^3-\frac{a^3\sqrt{3}}{9}\right)(1+tan\alpha)\right]\\+\frac{2}{3}a^2\left[\frac{\sqrt{3}}{9}\mu Fa(1-\delta_{pt})+\frac{\sqrt{3}}{9}\tau_{yield}A_s\delta_{pt}\right]+\frac{1}{2\pi}a^2L_p\left[\mu F(1-\delta_{ps})+\tau_{yeild}A_s\delta_{ps}\right]\end{array}\right] \quad (2)$$

2.2 Square pin profile

The energy per unit length of the weld for the flat shoulder tool is

$$Q'_{Energy}=\frac{\omega\eta_{fd}}{vR_s^2}\begin{bmatrix}\frac{2}{3}\left[\mu F\left(R_s^3-\frac{a^3\sqrt{2}}{4}\right)(1-\delta_{st})+\tau_{yield}A_s\delta_{st}\left(R_s^3-\frac{a^3\sqrt{2}}{4}\right)\right]\\+\frac{2}{3}\left[\mu F\frac{a^3\sqrt{2}}{4}(1-\delta_{pt})+\tau_{yield}A_s\delta_{pt}\frac{a^3\sqrt{2}}{4}\right]\\+\frac{1}{4\pi}a^2L_p\left[\mu F(1-\delta_{ps})+\tau_{yeild}A_s\delta_{ps}\right]\end{bmatrix} \tag{3}$$

The energy per unit length of the weld for the conical shoulder tool is

$$Q'_{Energy}=\frac{\omega\eta_{fd}}{vR_s^2}\begin{bmatrix}\frac{2}{3}\pi\left[\mu p\left(R_s^3-\frac{a^3\sqrt{2}}{4}\right)(1-\delta_{st})(1+tan\alpha)+\tau_{yield}\delta_{st}\left(R_s^3-\frac{a^3\sqrt{2}}{4}\right)(1+tan\alpha)\right]\\+\frac{2}{3}\pi\left[\mu p\frac{a^3\sqrt{2}}{4}(1-\delta_{pt})+\tau_{yield}\delta_{pt}\frac{a^3\sqrt{2}}{4}\right]+\frac{1}{4\pi}a^2L_p\left[\mu p(1-\delta_{ps})+\tau_{yeild}\delta_{ps}\right]\end{bmatrix} \tag{4}$$

2.3 Pentagonal pin profile

The energy per unit length of the weld for the flat shoulder tool is

$$Q'_{Energy}=\frac{\omega\eta_{fd}}{vR_s^2}\begin{bmatrix}\frac{2}{3}\mu F\left(R_s^3-0.6155a^3\right)(1-\delta_{st})+\frac{2}{3}\pi\tau_{yield}A_s\left(R_s^3-0.6155a^3\right)\\+\frac{2}{3}\pi\mu F(0.6155a^3)(1-\delta_{pt})+\frac{2}{3}\pi A_s\tau_{yield}(0.6155a^3)\delta_{pt}\\+1.8088\frac{a^2}{\pi}L_p\left[\mu F(1-\delta_{ps})+A_s\tau_{yield}\delta_{ps}\right]\end{bmatrix} \tag{5}$$

The energy per unit length of the weld for the conical shoulder tool is given

$$Q'_{Energy}=\frac{\omega\eta_{fd}}{vR_s^2}\begin{bmatrix}\frac{2}{3}\mu F\left(R_s^3-0.6155a^3\right)(1-\delta_{st})(1+tan\alpha)\\+\frac{2}{3}A_s\tau_{yield}\left(R_s^3-0.6155a^3\right)(1+tan\alpha)\\+\frac{2}{3}\mu F(0.6155a^3)(1-\delta_{pt})+\frac{2}{3}A_s\tau_{yield}(0.6155a^3)\delta_{pt}\\+1.8088\frac{a^2}{\pi}L_p\left[\mu F(1-\delta_{ps})+A_s\tau_{yield}\delta_{ps}\right]\end{bmatrix} \tag{6}$$

2.4 Hexagonal pin profile

The energy per unit length of the weld for the flat shoulder tool is developed as

$$Q'_{Energy}=\frac{\omega\eta_{fd}}{vR_s^2}\begin{bmatrix}\frac{2}{3}\left[\mu F\left(R_s^3-a^3\right)(1-\delta_{st})+A_s\tau_{yield}\left(R_s^3-a^3\right)\right]\\+\frac{2}{3}\mu Fa^3(1-\delta_{pt})+\frac{2}{3}\pi A_s\tau_{yield}a^3\delta_{pt}\\+3\frac{a^2}{\pi}L_p\left[\mu F(1-\delta_{ps})+A_s\tau_{yield}\delta_{ps}\right]\end{bmatrix} \tag{7}$$

The energy per unit length of the weld for the conical shoulder tool is given as

$$Q'_{Energy}=\frac{\omega\eta_{fd}}{vR_s^2}\begin{bmatrix}\frac{2}{3}\left[\mu F\left(R_s^3-a^3\right)(1-\delta_{st})(1+tan\alpha)+A_s\tau_{yield}\left(R_s^3-a^3\right)(1+tan\alpha)\right]\\+\frac{2}{3}\mu Fa^3(1-\delta_{pt})+\frac{2}{3}A_s\tau_{yield}a^3\delta_{pt}+3\frac{a^2}{\pi}L_p\left[\mu F(1-\delta_{ps})+A_s\tau_{yield}\delta_{ps}\right]\end{bmatrix} \tag{8}$$

Where in all the profile considered, the contact shear stress is given by

$$\tau_{cont} = \begin{cases} \mu p & \text{for frictional heat generation (Coulumb's friction law)} \\ \tau_{yield} & \text{for deformational heat generation} \end{cases} \quad (9)$$

where μ is the frictional coefficients, p is the contact pressure, τ_{yield} is the yield strength of the workpiece. Following Arora *et al.* [17], frictional coefficients can be calculated as

$$\mu = \mu_o exp\left(-\delta_{slip}\frac{\omega}{\omega_o}\frac{R_p}{R_s}\right) \quad (10)$$

where μ_o is the static friction coefficient and it is taken as 0.45 [18, 19]. δ_{slip} is the slipping factor, ω is the rotating speed and the reference rotation speed ω_o is taken as 400 rpm. R_p and R_s are the radii of the tool pin and the shoulder, respectively. The parameter η_{fd} represents the fraction of the mechanical energy that is converted to frictional heat and deformational heat. Which could be as high as 0.99 based on the assumptions of previous work. The boundary value of the yield shear stress from the von Misses yield criterion in uniaxial tension and pure shear is given by

$$\tau_{yield} = \frac{\sigma_{yield}(T,\varepsilon)}{\sqrt{3}} \quad (11)$$

The yield strength of the workpiece's material, $\sigma_{yield}(T,\varepsilon)$ is highly dependent on temperature, T and strain rate, ε. The analysis of the tangential stresses within FSW requires the full temperature and strain history in the workpiece in a wide zone around the welding tool. Sheppard and Wright [20] elastic-plastic model may be used to evaluate the temperature-strain dependent yield strength of the workpiece's material, $\sigma_{yield}(T,\varepsilon)$.

$$\sigma_{yield}(T,\varepsilon) = \frac{1}{\alpha}sinh^{-1}\left[\left(\frac{Z(\varepsilon,\mathrm{T})}{A}\right)^{\frac{1}{n}}\right] \quad (12)$$

where A, α, and n are material constants and Z(ε,T) is the Zener-Hollomon parameter that represents the temperature-compensated effective strain rate by

$$Z(\varepsilon,T) = \dot{\varepsilon}e\,\mathrm{xp}\left(\frac{Q}{RT}\right) \quad (13)$$

where $\dot{\varepsilon}, Q, R,$ and T are strain rate, activation energy, universal gas constant and absolute temperature, respectively. While Sheppard and Jackson [21] developed the elastic-plastic model for yield strength of the workpiece's material as

$$\sigma_{yield}(T,\varepsilon) \approx \frac{1}{\alpha}In\left\{\left(\frac{Z(T,\varepsilon)}{A}\right)^{\frac{1}{n}} + \left[1+\left(\frac{Z(T,\varepsilon)}{A}\right)^{\frac{2}{n}}\right]^{\frac{1}{2}}\right\} \quad (14)$$

It was stated that the lack of the detailed material constitutive information and other thermal and physical properties at conditions such as very high strain rates and elevated temperatures seems to be the limiting factor while modeling the FSW process [22]. Consequently, Colegrove and Sherchiff [23] and Wang *et al.,* [24] pointed out that Sheppard and Jackson's elastic-plastic model is not applicable at the melting of the material. Although, Su *et al.* [25] modified the Sheppard and Jackson's elastic-plastic model as

$$\sigma_{yield}(T,\varepsilon) = \sigma_o + \left\{\frac{1}{\alpha}\left(1-\sqrt{\frac{T-273}{T-273}}\right)In\left\{\left(\frac{Z(T,\varepsilon)}{A}\right)^{\frac{1}{n}} + \left[1+\left(\frac{Z(T,\varepsilon)}{A}\right)^{\frac{2}{n}}\right]^{\frac{1}{2}}\right\}\right\} \quad (15)$$

In this work, we adopt a developed generic model [26]:

$$\sigma_{yield}(T,\varepsilon) = \sigma_o + \left\{\frac{1}{\alpha}\left(1-\sqrt[p]{\frac{T-T_{room}}{T-T_{room}}}\right)In\left\{\left[\frac{\dot{\varepsilon}}{A}e\,\mathrm{xp}\left(\frac{Q}{RT}\right)\right]^{\frac{1}{n}} + \left[1+\left[\frac{\dot{\varepsilon}}{A}e\,\mathrm{xp}\left(\frac{Q}{RT}\right)\right]^{\frac{2}{n}}\right]^{\frac{1}{2}}\right\}\right\} \quad (16)$$

Where T_{room} is the room temperature and p is the model constant which ranges from $1.8 \le p \le 2.2$, depending on the material. σ_o is the yield stress beyond the melting point of the material. Alternatively, we have [26]

$$\sigma_{yield}(T,\varepsilon)=\sigma_o+\frac{1}{\alpha}\left\{\left(1-\sqrt[p]{\frac{T-T_{room}}{T-T_{room}}}\right)\sum_{p=1}^{\infty}(-1)^{p+1}\left(\frac{\dot{\varepsilon}}{A}e\,\mathrm{xp}\left(\frac{Q}{RT}\right)\right)^{2p-1}\frac{\prod_{p=1}^{\infty}(2p-1)}{\prod_{p=1}^{\infty}2p(2p+1)}\right\}\quad for\quad \left|\left(\frac{\dot{\varepsilon}}{A}e\,\mathrm{xp}\left(\frac{Q}{RT}\right)\right)\right|<1 \tag{17}$$

On expanding Eq. (17), we have

$$\sigma_{yield}(T,\varepsilon)=\sigma_o+\frac{1}{\alpha}\left(1-\sqrt[p]{\frac{T-T_{room}}{T-T_{room}}}\right)\left\{\begin{array}{l}\left(\frac{\dot{\varepsilon}}{A}e\,\mathrm{xp}\left(\frac{Q}{RT}\right)\right)^{\frac{1}{n}}-\frac{1}{6}\left(\frac{\dot{\varepsilon}}{A}e\,\mathrm{xp}\left(\frac{Q}{RT}\right)\right)^{\frac{3}{n}}+\frac{3}{40}\left(\frac{\dot{\varepsilon}}{A}e\,\mathrm{xp}\left(\frac{Q}{RT}\right)\right)^{\frac{5}{n}}\\ -\frac{5}{112}\left(\frac{\dot{\varepsilon}}{A}e\,\mathrm{xp}\left(\frac{Q}{RT}\right)\right)^{\frac{7}{n}}+\frac{35}{1152}\left(\frac{\dot{\varepsilon}}{A}e\,\mathrm{xp}\left(\frac{Q}{RT}\right)\right)^{\frac{9}{n}}\end{array}\right\} \tag{18}$$

Another generic model developed by the author [26] is

$$\sigma_{yield}(T,\varepsilon)=\sigma_o+\frac{1}{\alpha}\left\{\frac{1}{n}In\left(\left(\frac{2\dot{\varepsilon}}{A}e\,\mathrm{xp}\left(\frac{Q}{RT}\right)\right)\right)+\sum_{m=1}^{\infty}(-1)^{m+1}\frac{(2m)!\left(\left(\frac{\dot{\varepsilon}}{A}e\,\mathrm{xp}\left(\frac{Q}{RT}\right)\right)\right)^{-2m}}{2^m(m!)^2 2m}\right\}\quad for\quad \left|\left(\frac{\dot{\varepsilon}}{A}e\,\mathrm{xp}\left(\frac{Q}{RT}\right)\right)\right|>1 \tag{19}$$

which when expanded, we have

$$\sigma_{yield}(T,\varepsilon)=\sigma_o+\frac{1}{\alpha}\left(1-\sqrt[p]{\frac{T-T_{room}}{T-T_{room}}}\right)\left\{\begin{array}{l}\frac{1}{n}In\left(\frac{2\dot{\varepsilon}}{A}e\,\mathrm{xp}\left(\frac{Q}{RT}\right)\right)+\frac{1}{4}\left(\frac{\dot{\varepsilon}}{A}e\,\mathrm{xp}\left(\frac{Q}{RT}\right)\right)^{\frac{-2}{n}}\\ -\frac{3}{32}\left(\frac{\dot{\varepsilon}}{A}e\,\mathrm{xp}\left(\frac{Q}{RT}\right)\right)^{\frac{-4}{n}}+\frac{5}{96}\left(\frac{\dot{\varepsilon}}{A}e\,\mathrm{xp}\left(\frac{Q}{RT}\right)\right)^{\frac{-6}{n}}\\ -\frac{35}{1024}\left(\frac{\dot{\varepsilon}}{A}e\,\mathrm{xp}\left(\frac{Q}{RT}\right)\right)^{\frac{-8}{n}}+\frac{63}{2560}\left(\frac{\dot{\varepsilon}}{A}e\,\mathrm{xp}\left(\frac{Q}{RT}\right)\right)^{\frac{-10}{n}}\end{array}\right\} \tag{20}$$

However, in the analysis of heat generation in FSW, the influence of strain on the decrease of yield strength can be neglected and sufficient precision will still be maintained [27]. Neglecting strain effects on the yield strength is possible since the maximal temperatures of the material reach about 80% of the melting temperature when the strain has significant values due to near melting conditions in the material [17, 28]. Therefore, Eq. (13) becomes

$$\tau_{yield}=\frac{\sigma_{yield}(T)}{\sqrt{3}} \tag{21}$$

For Stainless steel, yield stress as developed in this work, we have

$$\sigma_{yield}(T)=\beta_o+\beta_1T+\beta_2T^2+\beta_3T^3++\beta_4T^4++\beta_5T^5 \tag{22-a}$$

where

$$\begin{aligned}&\beta_o=240,\ \beta_1=7.3583\times10^{-1},\quad \beta_2=-7.1333\times10^{-2},\quad \beta_3=2.163\times10^{-5},\\ &\beta_4=-2.7292\times10^{-8}\ and\quad \beta_5=1.1849\times10^{-8}\end{aligned} \tag{22-b}$$

3. Modeling the peak temperature in friction stir welding

The published works in literature point to the fact that there is an optimum temperature range to obtain defect-free joints and such a range has not been specified. However, a number of researchers as shown that there is a linear regression of the temperature ratio T_{peak}/T_s (where *Tpeak* is the peak/maximum temperature and Ts is the solidus temperature) on T_s was derived: where this temperature range can be thought of as the optimum temperature range, i.e. $T_{peak} = T_{opt}$. The correlation has a standard deviation of 0.024. The calculation results in a temperature range $T_{opt} = (0.8–0.9)\ T_s$. The rationality of this assumption was verified by experiments [28]. The linear relationship is given by:

$$\frac{T_{peak}}{T_s}=\frac{T_{opt}}{T_s}=\psi_1+\psi_2T_s \tag{23}$$

which gives

$$T_{peak} = (\psi_1 + \psi_2 T_s) T_s \tag{24}$$

where ψ_1 and ψ_2 are to be determined from experiment e.g. for Aluminum alloy 1100-H14 and 2024-T3 rolled plates 8 and 3.2 mm in thick, $\psi_1 = 1.344$ and $\psi_2 = 0.0005917$. Therefore, for the alloys

$$\frac{T_{peak}}{T_s} = \frac{T_{opt}}{T_s} = 1.344 + 0.005917 T_s \tag{25}$$

Also, empirical model developed by Hamilton et al. [14] shown in Eq. (26) could be adopted

$$\frac{T_{peak}}{T_s} = 0.54 + 0.000156\,\mathrm{Q}_{max} \tag{26}$$

and Essa et al. [15]:

$$\frac{T_{peak}}{T_s} = 0.5 + 0.0002\,\mathrm{Q}_{max} \tag{27}$$

where

$$\mathrm{Q}_{max} = \varphi\,\mathrm{Q}_{Energy} \tag{28}$$

φ is the ratio of the pin length L_p to the workpiece thickness, t. In this work, our analysis establishes a non-linear regression of the peak temperature and maximum heat generation, Q_{max}

$$T_{peak} = \xi(\mathrm{Q}_{max}\,\bar{\mathrm{Q}})^{\gamma} \tag{29}$$

Also, $\bar{\mathrm{Q}}$ is the non-dimensional heat input, which is defined as [30]:

$$\bar{\mathrm{Q}} = \frac{\sigma_8 S \omega C \eta}{k_w v^2} \tag{30}$$

where, for conformity of calculation, the unit of ω changes from rpm to rad m/s and v from mm/min to m/s, σ_8 is the yield stress of the material at a temperature of $0.8T_S$, S is the cross-sectional area of the tool shoulder, C is the specific heat capacity of the workpiece material, k_w is the thermal conductivity of the workpiece, and η is the ratio according to which heat generated at the shoulder–workpiece interface is transported between the tool and the workpiece, and is defined as:

$$\eta = \frac{\sqrt{(k\,\rho c_p)_w}}{\sqrt{(k\,\rho c_p)_T}} \tag{31}$$

also

$$v = \frac{\pi N r}{30 n \alpha \sigma_{yield}(T, \varepsilon)} \tag{32}$$

On substituting Eq. (32) into Eq. (30), we arrived

$$\bar{\mathrm{Q}} = \frac{\sigma_8 S \left(\frac{\pi N}{30}\right) C \eta}{k_w \left\{\frac{\pi N r}{30 n \alpha \sigma_{yield}(T, \varepsilon)}\right\}^2} \tag{33}$$

Substituting Eq. (33) into Eq. (28) and (29), the peak temperature is developed as

$$T_{peak} = \xi \left\{ \varphi \mathrm{Q}'_{Energy} \frac{\sigma_8 S \left(\frac{\pi N}{30}\right) C \eta}{k_w \left\{\frac{\pi N r}{30 n \alpha \sigma_{yield}(T, \varepsilon)}\right\}^2} \right\}^{\gamma} \tag{34}$$

4. Results and Discussion

Fig. 2 shows the effects of tool pin geometry on the total heat generation rate at the interfaces. From the results, it is depicted that by increasing the number of edges, the amount of heat generation initially increases from the square

pin to hexagonal pin profile and then decreases to the triangular pin profile. Furthermore, increasing the tool rotational speed under constant weld speed, heat input increases, and increasing the weld speed under constant tool rotational speed, heat input decreases. For the experimental conditions studied by Ramanjaneyulu *et al.* [8], the results show that the heat generation and the peak temperature is directly proportional to the number of edges on the pin profile i.e. the heat generation and the peak temperature increase from pin with triangular profile (three edges) to pin with hexagonal profile (six edges). The peak temperature at a given point is experienced by the point shortly after it is passed by the heat source. It is useful for estimating the heat-affected zone size and also for showing the effect of preheat on the HAZ size. It is evident from the equations that all parameters being constant, preheating increases the size of the HAZ. Also, the size of the HAZ is proportional to the net energy input. Thus, the high-intensity processes have a smaller HAZ. A high intensity energy source results in a lower total heat input because the energy used in melting the metal is concentrated in a small region.

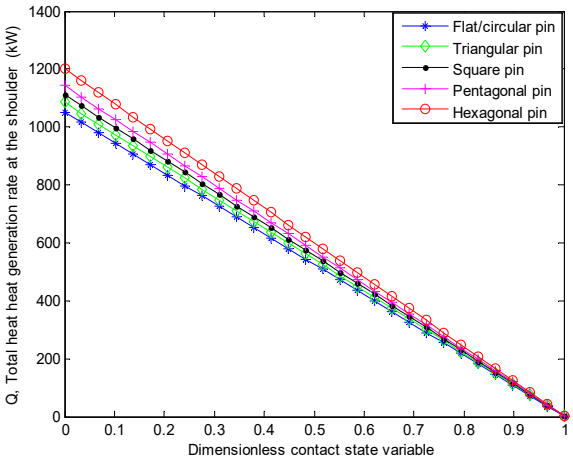

Fig. 2. Effects of pin shape on the total heat generation rate at the interfaces

Figs. 3-8 show the effects of welding speed, rotation speed and the efficiency of heating on the peak temperature of the workpiece. Fig. 3 shows variation of peak temperature with welding rotational speed at different welding velocities while Fig. 4 shows the variation of peak temperature with welding velocity at different power efficiency factors. The figure indicates that the peak temperature decreases with increase in welding velocity while it increases with rotational speed. This behavior originates from the fact that at higher welding velocity, the heat input per unit length decreases and heat is dissipated over a wider region of the workpiece. It is also observed that peak temperature becomes higher with higher power efficiency factors, as expected.

Also, peak temperature increases with increase in rotational velocity and power efficiency factor as shown in Fig. 4. At high rotational speed, the relative velocity between the tool and workpiece is high, and consequently the heat generation rate and the temperatures are also high. The spread in the data in this figure is due to the fact that the tool rotational speed is not constant as the welding speed varies. It can be seen, however, that predicted maximum temperatures tend to decrease as the translational speed increases. While increasing the welding speed tends to decrease the maximum temperature, increasing the rotational speed has the opposite effect; and this can be observed in Fig. 3. It may be noted here that the peak temperatures in four locations are in the range of about 790 to 807 K depending on the welding velocity and rotational speed. The peak temperatures close to the centerline are similar but decrease with distances away from the tool. The tool is like a heat source; thereby distances away from the tool are expected to be at lower temperature.

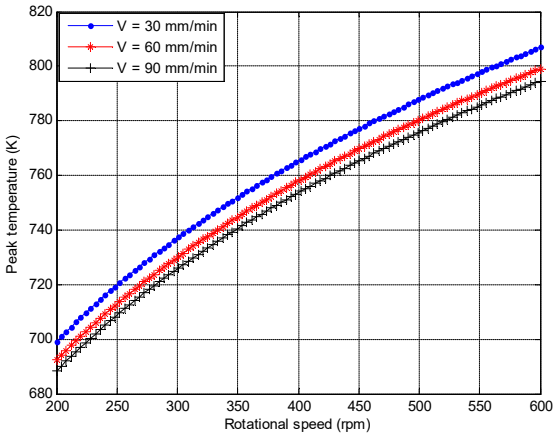

Fig. 3. Effects of welding velocity on the peak temperature as variation of rotational speed

Figs. 4 shows the variation of peak temperature with welding speed at different power efficiency factors of 0.85, 0.90 and 0.95. The figure indicates that the peak temperature decreases with increase in welding velocity. This is because at higher welding velocity, the heat input per unit length decreases and heat is dissipated over a wider region of the workpiece. Unsurprisingly, the peak temperature becomes higher with higher power efficiency factors. Also, the figures show the effects of heat generation at the shoulder on the welding speed. As expected, as the welding speed increases, the heat generation at the shoulder increases. This is because, the increase in the speed of the welding tool causes more agitation in the workpiece, increases the random motion and collisions of the workpiece particles and in consequent, more heat are generated.

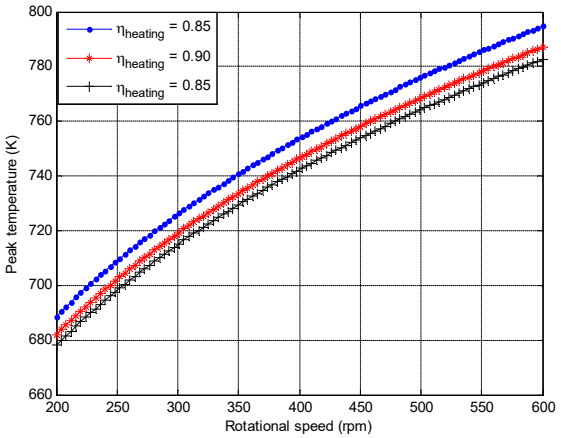

Fig. 4. Effects of efficiency of heating on the peak temperature as variation of rotational speed

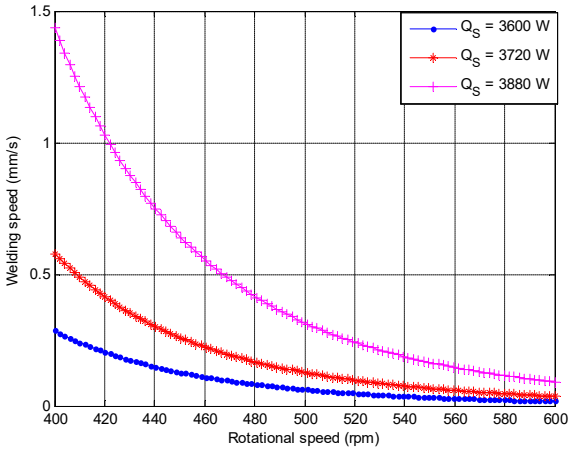

Fig. 5. Effects of heat generation at the shoulder on the welding speed as variation of rotational speed

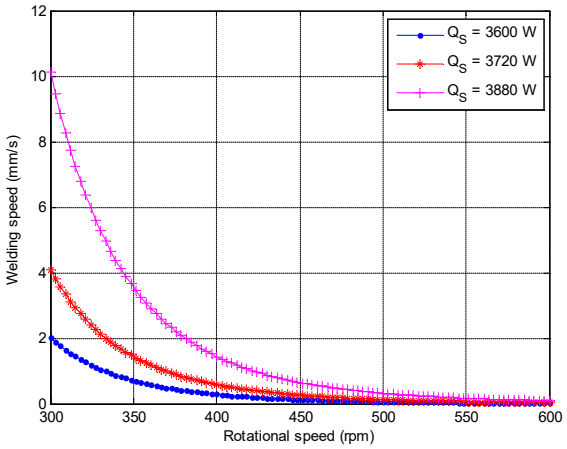

Fig. 6. Effects of heat generation at the shoulder on the welding speed as variation of rotational speed

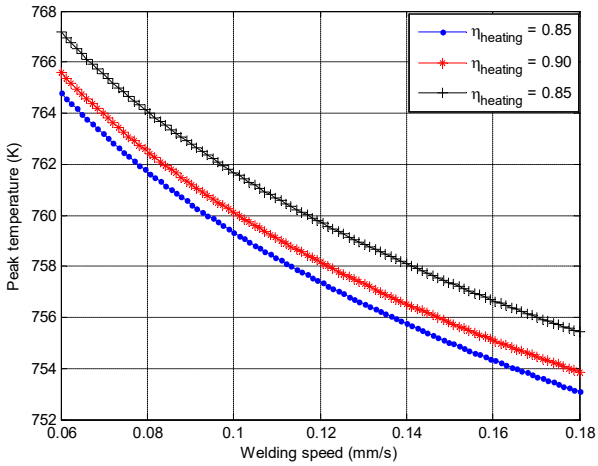

Fig. 7. Effects of efficiency of heating on the peak temperature as variation of welding speed

Fig. 8 shows the variation of peak temperature with welding speed at different rotational speed. The peak temperature increases with increase in rotational velocity. At high rotational speed, the relative velocity between the tool and workpiece is high, and consequently the heat generation rate and the temperatures are also high. Although the peak temperature decreases with increase in welding speed, as the rotational speed of the tool increases, the peak temperature increases. These trends or effects is occurred because, the increase in the rotational speed of the welding tool as it is inserted into the workpiece causes more agitation in the workpiece, increases the random motion and collisions of the workpiece particles and in consequent, more heat are generated and therefore the peak temperature of the tool increases. It should be noted that the higher tool traverse speed induces a lower heat input to the weld zone; the rotary speed determines the quality of heat production and degree of plastic deformation. The traverse speed determines the heat input per unit length of the weld. At higher rotary speed, the peak temperature is higher and forms lots of plastic metal. With the increase of temperature, thermal activation energy provides lots of energy to the dislocation motion and significant residual stress relaxation is likely to occur. Moreover, there is enough time for the stress relaxation due to long cooling times. At lower traverse speed, i.e., higher heat input per unit length, material further away from the weld line is heated up; this results in an increase in the width of the high temperature zone around the tool and a decrease of thermal gradients, thus reducing the thermal expansion mismatch upon cooling, which has been previously observed in the literature [21].

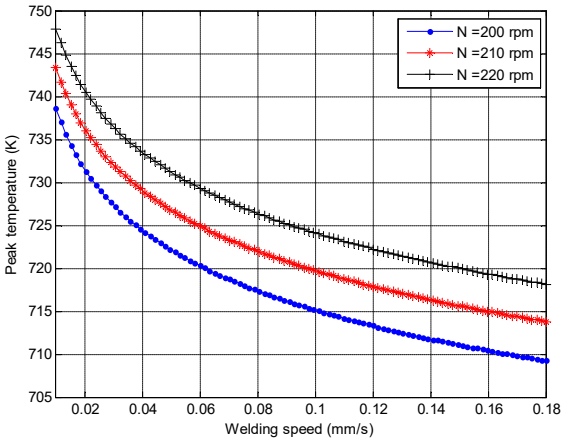

Fig. 8. Effects of rotational speed on the peak temperature as variation of welding speed

Table 1. Comparison of results of heat generated and peak temperature for different tool profiles

Profile	Q_{Eff} J/mm [8]	Q_{Eff} J/mm (Present work)	$T_{peak}(K)$ Experiment [8]	$T_{peak}(K)$ Numeric [4]	$T_{peak}(K)$ Analytic [4]	$T_{peak}(K)$ (Present work)
Triangle	163.25	393.19	614	733	515	547
Square	167.70	429.64	619	789	516	553
Pentagon	135.63	471.88	623	724	511	559
Hexagon	121.01	514.40	637	713	509	565

For the experimental conditions studied by Ramanjaneyulu *et al.* [8], the results show that the heat generation and the peak temperature is directly proportional to the number of edges on the pin profile i.e. the heat generation and the peak temperature increase from pin with triangular profile (three edges) to pin with hexagonal profile (six edges).

Apart from the fact that our present study establishes this experimental fact analytically, which are not well established by the analytical results of Gadakh *et al*. [4], judging from the established experimental results as stated in Table 1, our present study have better predictions for the peak temperature than the previous analytical study as shown in Table 1. The enhanced predictions are due to the improved models developed in this present work.

5. Conclusion

In this work, analytical models have been developed to investigate the effects of different tool pin profiles of flat and tapered shoulder geometries on the peak temperature in friction stir welding. The results showed that the amount of heat generation and the peak temperature are directly proportional to the number of edges in the pin profiles in such a way that the heat generated and peak temperature in the profiles increases from the triangular pin profile to hexagonal pin profile. Also, the rate of heat generation and the peak temperature in flat shoulder are greater than in tapered/conical shoulder. The results in this work have been validated with experimental and the past theoretical results and good agreements were achieved.

References

[1] Chao, Y. J., Qi, X. Tang, W. Heat transfer in friction stir welding: experimental and numerical studies, ASME J. *Manuf. Sci. Eng*., 125, 138–145, 2003.

[2] Frigaard, O., Grong, O., Midling, O. T. A process model for friction stir welding of age hardening aluminium alloys. *Metall. Mater. Trans. A.* 32, 1189–1200, 2001.

[3] Russell, M. J., Shercliff, H. R., *1st Int. Symp. on Friction Stir Welding,* Thousand Oaks, California, USA,1999.

[4] Gadakh, V. S., Kumar, A., Patil, J.V. Analytical Modeling of the Friction Stir Welding Process using Different Pin Profiles. *Welding Research*, 94(4), 115-124, 2015.

[5] Colegrove, P.A., Shercliff, H.R., Zettler, R. A model for predicting the heat generation and temperature in friction stir welding from the material properties. *Sci. Technol. Weld. Joining*, 12, 284–297, 2007.

[6] Raouche, E., Driss, Z., Guidara, M., Khalfallah, F. Effects of the tool geometries on the thermal analysis of the friction stir welding. *International Journal of Mechanics and Applications*, 6(1), 1-7, 2016.

[7] Emamikhah, A. Abbasi, A., Lirabi, I., Feghhi, Amir, Atefat, A. The role of tool pin profile and temperature on friction stir welding of high zinc brass. *Advanced Material Research*, 685, 264-268, 2013.

[8] Ramanjaneyulu, K., Reddy, M., Rao, V., Markandeya, R. Structure-Property Correlation of AA2014 Friction Stir Welds: Role of Tool Pin Profile. *JMEPEG*, 22, 2224-2240, 2013.

[9] Juárez, J.C.V., Almaraz, G.M.D, Hernández, R.G., López, J. J. V. Effects of Modified Pin Profile and Process Paramters on the Friction Stir Welding of Aluiminium Alloy 6061-T6. *Advances in Material Science and Engineering*, Vol 2016, 7567940, 9pages.

[10] Yatapu, Y. R., Reddy, B. R., Ramaraju, R. V., Ku, M. F. B. C., Ibrahim, A. B. Prediction of Temeperatures during Friction Stir Welding of AA6061 Aluminium Alloy using Ayperworks. *ARPN Journal of Engineering and Applied Sciences*, 11(18), 11003-11008, 2016

[11] Patil, M. S., Msatud, S. A. Simulation and Calculation of Peak Temperature in Friction Stir Welding Process of Aluminium Plates. *International Journal of Science Technology and Enginering*, 2(1), 6-12, 2015.

[12] Patel, J. B., Patil, H. S. Simulation of Peak Temperature and Flow Stress during FSW of Aluminium Alloy AA6061 for various Tool Pin Profiles. *International Journal of Material Science and Engineering*, 2(1), 67-71, 2014.

[13] Manvatur, V., De, A., Svensson, L-E, T. DebRoy. Cooling Rates and Peak Temperatures during Friction Stir Welding of High-Carbon Steel. *Scripta Materialia*, 94, 36-39, 2015.

[14] Hamilton, C., Dymek, S., Sommers, A. A Thermal Model of Friction Stir Welding in Aluminium Alloys. *Int. Journal of Machine Tools Manuf.*, 48, 1120-1130, 2008.

[15] Essa, A. R. S., Ahmed, M. M. Z., Mohamed, A. Y. A., El-Nikhaily, A. E. An Analytical Model of Heat Generation for Eccentric Cylindrical Pin in Friction Stir Welding. *Journal of Materials Research and Technology*, 5(3), 234-240, 2016.

[16] Waheed, M.A., Jayesimi, L.O., Ismail, S.O., Dairo, O.U. Modeling of Heat Generations for Different Tool Profiles in Friction Stir Welding: Study of Tool Geometry and Contact Conditions. *Journal of Applied and Computational Mechanics*. 3(1), 37-59, 2017.

[17] Arora, A., Nandan, R., Reynolds, A.P., Debroy, T. Torque, power requirement and stir zone geometry in friction stir welding through modeling and experiments. *Scripta Mater*, 60, 13–16, 2009.

[18] El-Tayeb, N.S.M., Low, K.O., Brevern, P.V. On the surface and tribological characteristics of burnished cylindrical Al-6061. *Tribol. Int.*, 42, 320–326, 2009.

[19] Devaraju, A., Kumar, A., Kotiveerachari, B. Influence of addition of Grp/Al2O3p with SiCp on wear properties of aluminum alloy 6061-T6 hybrid composites via friction stir processing. *Trans Nonferrous Met Soc China*, 23, 1275–1280, 2013.

[20] Sheppard, T., Wright, D. Determination of flow stress. Part 1 constitutive equation for aluminum alloys at elevated temperatures, *Met. Technol.*, 6, 215–223, 1979.

[21] Sheppard, T., Jackson, A. Constitutive equations for use in prediction of flow stress during extrusion of aluminium alloys, *Materials Science and Technology*, 13(3), 203–209, 1997.
[22] Uyyuru, R.K., Kallas, S.V. Numerical analysis of friction stirs welding process. *J. Mater. Eng. Perform.*, 15, 505–18, 2006.
[23] Colegrove, P.A., Shercliff, H.R. CFD Modelling of the friction stir welding of thick Plate 7449 aluminium alloy. *Sci. Technol. Weld. Joining*, 11 (4), 429–441, 2006.
[24] Wang, H., Colegrove, P.A., Dos Santos, J.F. Numerical investigation of the tool contact condition during friction stir welding of aerospace aluminium alloy. *Comput Mater Sc*i., 7, 101–108, 2013.
[25] Su, H., Wu, C., Chen, M. Analysis of material flow and heat transfer in friction stir welding of aluminium alloys. *China Weld (Engl Ed)*, 22, 6–10, 2013.
[26] Sobamowo, M. G. New models for the prediction of temperature-strain dependent flow stress during machining and fabrication of material. Report on Improved models for flow stress predictions. Unpublished Work, 2016.
[27] Schmidt, H., Hattel, J., Wert, J. An analytical model for the heat generation in friction stir welding. *Modelling Simul. Mater. Sci. Eng.* 12, 143–157, 2004.
[28] Khandkar, M. Z. H., Khan, J. A., Reynolds, A. P. Prediction to temperature distribution and thermal history during friction stir welding: Input torque based model. *Sci. Technol. Weld. Join.*, 8, 165–174, 2003.
[29] Qian, J. Li, J. Sun, F., Xiong, J. Zhang, F., Lin, X. An analytical model to optimize rotation speed and travel speed of friction stir welding for defect-free joints. *Scriptia Materialia*, 68, 175-178, 2013.
[30] Roy, G. G., Nandan, R. and DebRoy, T. Dimensionless correlation to estimate peak temperature during friction stir welding. *Sci Technol Weld Join*, 11, 606–608, 2006.
[31] Lombard, H., Hattingh, D. G., Steuwer, A. and James, M. N. Effect of process parameters on the residual stresses in AA5083-H321 friction stir welds. *Mater Sci Eng A*. 501(1-2), 119-124, 2009.